Atmospheric Research 233 (2020) 104699

Contents lists available at ScienceDirect

Atmospheric Research

journal homepage: www.elsevier.com/locate/atmosres

Temporal variation and long–range transport of gaseous elemental mercury (GEM) over a coastal site of East China

Hui Yi[a,b,c,1], Lei Tong[a,c,1], Jia-mei Lin[a,b,c], Qiu-liang Cai[a,b,c], Ke-qiang Wang[a,b,c], Xiao-rong Dai[a,c], Jian-rong Li[a,c], Jin-sheng Chen[a,c], Hang Xiao[a,c,*]

[a] Center for Excellence in Regional Atmospheric Environment & Key Lab of Urban Environment and Health, Institute of Urban Environment, Chinese Academy of Sciences, Xiamen 361021, China
[b] University of Chinese Academy of Sciences, Beijing 100049, China
[c] Ningbo Urban Environment Observation and Research Station, Chinese Academy of Sciences, Ningbo 315800, China

ARTICLE INFO

Keywords:
GEM
Temporal variation
K-means clustering
Backward trajectory
Concentration weighted trajectory (CWT)

ABSTRACT

Continuous measurements of gaseous elemental mercury (GEM) play a key role in identifying mercury sources and its behavior in the atmosphere. In order to investigate the characteristics of GEM during the year when Minamata Convention on Mercury has entered into force in China, concentrations of GEM along with other pollutants were continuously measured at a coastal site in Ningbo, China. Hourly mean concentration of GEM at the study site ranged from 0.64 to 13.58 ng m^{-3} and showed an annual mean of 2.44 ± 0.95 ng m^{-3}. The atmospheric GEM showed obvious seasonal variations, with the highest seasonal average concentration in winter (2.62 ± 1.05 ng m^{-3}) and the lowest value in summer (2.26 ± 0.78 ng m^{-3}). The monthly variation of GEM/TGM ratios ranged from 72.6% to 98.0% and clear inverse trends for monthly GEM/TGM and O_3 were found during the entire period. Higher O_3 concentration promote the photochemical oxidation of GEM into divalent mercury. Additionally, a high GEM episode that lasted > 3 days was analyzed, and it showing high correlation with $PM_{2.5}$ and SO_2. The dilution of marine airflow and enhanced oxidation of GEM over sea are important for GEM depletion at the coastal site. Smoothed concentration weighted trajectory (CWT) analysis revealed that the GEM at the study site was mainly impacted by anthropogenic emissions from coastal provinces (Fujian, Jiangsu and Zhejiang) and inland provinces (Jiangxi, Anhui and Hubei). Coordinated inter-regional control on pollutant emissions is essential for the mercury reduction in the study area.

1. Introduction

Mercury brings significant negative effects on ecological balance and human health due to its high bio-accumulative, ubiquitous, and hypertoxic properties. It is capable of entering human bodies through respiration tract and cause damages to human organs such as gastro-intestinal ulcer, diarrhea, pulmonary edema, respiratory failure, and neuropsychiatric symptom. Globally, anthropogenic emission of total atmospheric mercury is 2050 Mg a^{-1}, including 1950 Mg a^{-1} total gaseous mercury (TGM) (Holmes et al., 2010). TGM accounts for the main component of total atmospheric mercury; and it can be classified into two classes: gaseous elemental mercury (GEM) and gaseous oxidized mercury (GOM), i.e., TGM = GEM + GOM. Due to its high stability and volatility, GEM is the predominant form of atmospheric mercury. With a relatively long atmospheric lifetime about 6–24 months, GEM can undergo long-range transport and plays a vital role in regional and global mercury circulation and transformation (Hall, 1995; Schroeder and Munthe, 1998; Steffen et al., 2005). GOM, typically originated from combustion processes or photochemical reactions, is composed of volatile species such as $HgBr_2$, $HgCl_2$, CH_3HgCl and $(CH_3)_2Hg$, and usually has a shorter atmospheric lifetime (several days to weeks) due to its high solubility and reactivity (Mastromonaco et al., 2016; Duan et al., 2017a; Duan et al., 2017b). As reported in previous studies (Fu et al., 2010; Wang et al., 2016; Duan et al., 2017b), GEM emitted from the natural or anthropogenic sources are mostly associated with transportation and transformation processes, which exhibit remarkable differences in different regions around the world. Long term measurements are essential to reveal the behaviors of regional atmospheric mercury and to identify the contributions of local and regional emission sources.

* Corresponding author at: Institute of Urban Environment, Chinese Academy of Sciences, 1799 Jimei Avenue, Xiamen 361021, China.
E-mail address: hxiao@iue.ac.cn (H. Xiao).
[1] The two authors contributed equally to this paper.

https://doi.org/10.1016/j.atmosres.2019.104699
Received 6 July 2019; Received in revised form 21 September 2019; Accepted 3 October 2019
Available online 17 October 2019
0169-8095/

Many lines of evidence, including estimates of anthropogenic and natural emission strengths, have strongly implied the post-industrial enhancement on the level of mercury in the atmospheric environment (Steffen et al., 2005). Currently, China has been undergoing rapid urbanization and industrialization, which has made China the largest mercury production and consumption country in the world. The national mercury emission increased from 448 to 2151 tons during the period of 1980–2012 in China (Ying et al., 2017). It is noteworthy that the average atmospheric mercury concentration displayed an increasing trend in recent years. Previous studies have showed that the average concentrations of GEM in Shanghai were 2.70 ng m^{-3} in 2009 and 4.19 ng m^{-3} in 2014, which are much higher than those at urban sites in Europe and North America and in rural areas of China, but lower than those at urban sites of China (Friedli et al., 2011; Choi et al., 2013; Duan et al., 2017b). Mean TGM concentrations were found to be 8.30 and 3.22 ng m^{-3} at urban and rural sites in Beijing, respectively (Liu et al., 2002), which are about 2–20 times higher than the background concentration of the Northern Hemisphere (Zhang et al., 2013). China has joined the Minamata Convention on Mercury on 28th April 2016, and it has come into force on 16th August 2017 in China. A series of mercury reduction measures have been implemented over the whole country such as technical innovation, enhanced efficiency, implementation of regulations on clean production and mercuric recycling (Ying et al., 2017). Investigating the specific characteristic of atmospheric mercury during the year when Minamata Convention on Mercury entered into force is essential to prevention and treatment of atmospheric mercury pollution in China.

This study was carried out in Ningbo, a port city in Yangtze River Delta region which located on the east coast of China. Ningbo has an area of 9816 km^2 and a dense population of 8.2 million. It is a highly industrialized city with GDP of 160.5 billion dollars in 2018. There are 18 coal-fired power plants here with the total consumptions of coal and crude oil being 36.7 and 29.1 million tons in 2017 (Ningbo Municipal Statistics Bureau, 2018). In this study, atmospheric GEM was monitored at a coastal site of Ningbo. The main objectives were to determine the temporal variation of GEM and its influencing factors, and to identify the potential sources of GEM during the year when Minamata Convention on Mercury has entered into force in China.

2. Materials and methods

2.1. Site description

Ningbo is a highly-industrialized city which located in the core zone of Yangtze River Delta (YRD) region with typical subtropical monsoon climate. The prevailing wind direction is southeast in summer, and northwest in winter. The average annual temperature, sunshine hours and precipitation of Ningbo City are 16.4 °C, 1850 h and 1480 mm, respectively. The rainy seasons are from March to June and August to September. The study site is located in the Urban Environment Observation and Research Station in Beilun, Ningbo, China (121°53′42.32″ E, 29°45′4.59″ N, height: 15 m, UTC + 8). As showed in Fig. 1, the station is located on the east coastal of China, immediately adjacent the East China Sea. An automobile assembling factory and a natural gas processing plant are in the vicinity of the monitoring station. Besides, a coal-fired power plant is located approximately 22 km in northwest of the station. The power plant is the third largest coal fire power plant in China with a total installed capacity of 5000 MW. With the implementation of environmental protection policies, a high-efficiency electrostatic precipitator, a limestone/plaster desulfurization system and a SCR denitrification facility with the ability of synergistic removal of mercury were gradually put into operation in this power plant in the years of 2006, 2007 and 2014, respectively. This have substantially reduced the pollutant emissions. A large-scale chlor-alkali plant is located 20 km in the northeast of station, it has been technological transformed with mercury-free technologies, which have significantly reduced the Hg emission to the atmosphere.

2.2. Measurement of GEM

Measurement campaign was conducted in the study site from 1st December 2016 to 30th November 2017. According to the research needs, GEM was continuously measured using a fully automated mercury analyzer (Tekran 2537A, Toronto, Canada) with a detection limit of 0.10 ng m^{-3} at a time resolution of 5 min. The analyzer includes a host machine (2537A) and several model units (1110, 1130). Model 1110 is an air purifier which produces zero air for calibration. The ambient air was drawn into the inlet port with a flow rate of 1.5 L min^{-1}, then GOM was trapped by a KCl-coated quartz annular denuder (1130). GEM was adsorbed onto a gold matrix and thermally released in an argon carrier gas stream and is detected by Cold Vapor Atomic Fluorescence Spectrometry (CVAFS). The system routinely underwent automated calibrations once a day using an internal permeation source which generates standard saturated mercury vapor (Liu et al., 2002). In order to determine the TGM concentration, GOM is also measured in this study (TGM = GEM + GOM). When the data are obtained, the outlier and invalid values are culled using the statistical method. A total of 46,019 and 1183 significant values for GEM (5 min resolution) and GOM (2 h resolution) were obtained for analysis. All the 5-min samples were transformed to hourly concentrations of mercury by averaging over 60-min periods.

2.3. Regular air pollutants and meteorological conditions

In order to better describe the mercuric transportation and transformation mechanisms in ambient air, concentrations of regular air pollutants such as NO_2 (Model 42i), O_3 (Model 49i), CO (Model 48i) and SO_2 (Model 43i) were measured using commercial available instruments from Thermo-Fisher Scientific Inc. (USA). Inhalable particulate matter (PM_{10}) and fine particulate matter ($PM_{2.5}$) were monitored using a tapered-element oscillating microbalance sampler (R&P TEOM, 1400). The TEOM sampler is regularly calibrated by using filters with measured masses. Zero and span checks are made every week. Meteorological parameters such as temperature (T), pressure (P), relative humidity (RH), wind direction (WD) and wind speed (WS) were measured by an automatic meteorological station (WS500-UMB, Lufft, Germany). The data collected at 5 min intervals were reported here as 1 h averages.

2.4. Bivariate polar analysis

Bivariate polar plot provides a graphical method for showing the joint wind direction, wind speed dependence of air pollutant concentration at a receptor site. The plots are constructed according to Carslaw and Beevers (2013). Original data are partitioned into wind direction-speed bins and mean GEM concentrations are calculated for each bin. Wind direction and speed intervals are at 10° and 2 m s^{-1}, respectively. The GEM concentrations are estimated by a Generalized Additive Model (GAM). In this study, wind speed is also substituted by SO_2 and $PM_{2.5}$ for further analysis. Polar coordinate is useful to reveal the directional dependence of sources and to identifying the source types and characteristics (Jones et al., 2010). It has been proved to be extremely valuable for identifying sources of air pollutants (Westmoreland et al., 2007).

2.5. k-Means clustering analysis

The emission sources of GEM were identified and clustered using a k-means clustering model. It is a kind of method with which bivariate polar plot features can be identified and grouped (Carslaw and Beevers, 2013; Chuang et al., 2018). Clusters are comprised of points separated by small Euclidean distances relative to the distance between clusters.

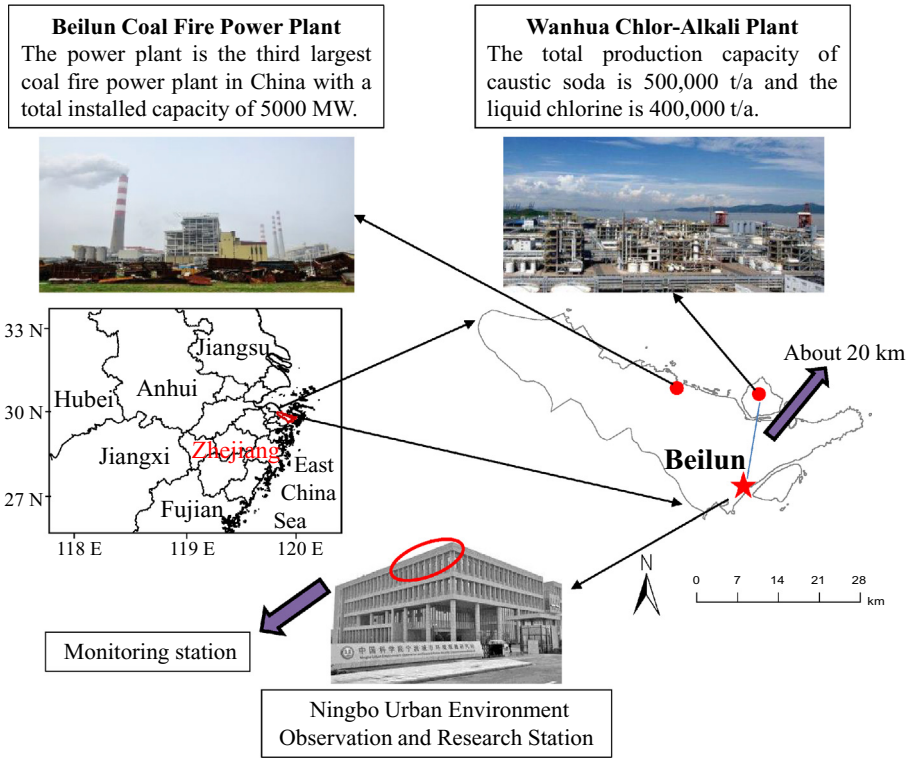

Fig. 1. Map of the monitoring station.

As we known, a bivariate polar plot is determined by a set of points $X = \{x_1, x_2, \ldots, x_n\}$. Each point has three variables: wind direction, wind speed and concentration. X is clustered into a new set of points C ($C = \{c_1, c_2, \ldots, c_k\}$). The basic algorithm for k clusters is obtained by minimizing Eq. (1) (Carslaw and Beevers, 2013):

$$\sum_{k=1}^{K} \sum_{x_i \in c_k} \|x_i - \mu_k\|^2 \tag{1}$$

where $\|x_i - \mu_k\|^2$ represents a chosen distance measure, μ_k represents the mean of cluster c_k. Acceptable cluster amount ranges from 2 to 10, and an optimal value was determined based on the environmental circumstance. K-means clustering is a novel way to identifying source characteristics. In this study, both bivariate polar plot and k-means clustering were performed using the R Statistical Software (R Studio, Version 1.1.463) (Carslaw and Ropkins, 2012; Carslaw and Beevers, 2013).

2.6. Backward trajectory and concentration weighted trajectory (CWT) analyses

Atmospheric GEM is influenced by local emission, regional and long-range transportation from the source region. In order to investigate the potential sources of GEM, 72 h' backward trajectory and concentration weighted trajectory (CWT) analysis are computed using the MeteoInfo software (Version: 1.4.9R2) (Wang et al., 2009). This software has a TrajStat plugin which is exclusively used to view, query and cluster the trajectories and compute the CWT. Before performing CWT analysis, hourly-resolved meteorological data for backward trajectories calculations were downloaded from NOAA ARL NCEP/NCAR Reanalysis FTP (Schneider et al., 2019). The calculated trajectories were converted to the ESRI shape file format, and then hourly averaged GEM data were assigned to the corresponding trajectories. The polluted trajectories with high GEM concentrations were identified by a build-in query function. A CWT layer with 0.4° × 0.4°cell size was created. Each grid cell was assigned a weighted concentration by Eq. (2).

$$c_{ij} = \frac{1}{\sum_{l=1}^{M} \tau_{ijl}} \sum_{l=1}^{M} c_l \tau_{ijl} \tag{2}$$

where c_{ij} is the average weighted concentration in the ijth cell, l is the index of the trajectory, M is the total trajectories, c_l is the GEM concentration observed on arrival of trajectory l, and τ_{ijl} is the time spent in the ijth cell by trajectory l. A high value for c_{ij} implies that air parcels traveling over the ijth cell would be associated with high concentrations at the receptor.

After the CWT values were calculated, they were multiplied by an arbitrary weight function W_{ij} (Eq. (3)) to reduce the uncertainty of cells with few endpoints (Polissar et al., 1999). The weighting function reduced the CWT values of some cells when the total number of the endpoints in a particular cell was less than about three times the average value of the end points per each cell. In a CWT diagram, high value for a grid cell implies that air parcels traveling over the grid cell would be associated with high concentrations at the receptor site.

$$W_{ij} = \begin{Bmatrix} 1.00 & 3.000N_{ave} < n_{ij} \\ 0.70 & 0.750N_{ave} < n_{ij} \le 3.000N_{ave} \\ 0.42 & 0.375N_{ave} < n_{ij} \le 0.750N_{ave} \\ 0.05 & 0.375N_{ave} \ge n_{ij} \end{Bmatrix} \tag{3}$$

where, n_{ij} is total number of endpoints in ijth cell, N_{ave} is the average number of the endpoints for all the cells.

3. Results and discussion

3.1. Atmospheric GEM concentrations

During the study period, the average GEM concentration at Beilun was 2.44 ± 0.95 ng m^{-3} with the range of 0.64 to 13.58 ng m^{-3}. The median value of GEM was 12% lower than the mean value and the 1st and 3rd quartiles lied in the range of 1.81–2.79 ng m^{-3}. GEM accounted for an average over 86% of the total gaseous mercury, lower than the value in Shanghai (97%) and Xiamen (93%) (Xu et al., 2015;

Table 1
Comparison of GEM at various locations around the world.

Country/region	Location	Character	GEM (ng/m^3)	Time period	Reference
Antarctic	Weddell Sea	Oceanic	0.77	2013.6–2013.10	(Mastromonaco et al., 2016)
Antarctic	McMurdo	Polar zone	0.94	2003.10–2003.11	(Brooks et al., 2008b)
Arctic	Alert	Polar zone	1.58	1995–2002	(Steffen et al., 2005)
Arctic	Amderma	Polar zone	1.65	2001	(Pankratov et al., 2013)
Canada	Kuujjuarapik	sub-Arctic	1.80	1998.8–2001.1	(Steffen et al., 2005)
Canada	Québec	Rural	1.65	2003	(Poissant et al., 2005)
USA	Dexter	Rural	1.59	2004	(Liu et al., 2010)
USA	New York	Forest	1.40	2006.6–2007.5	(Choi et al., 2008)
USA	New York	Rural	1.40	2007.12–2009.11	(Choi et al., 2013)
Ireland	Mace Head	Rural	1.77	1995–2001	(Ebinghaus et al., 2001)
Korea	Seoul	Urban	3.22	2005.2–2006.2	(Kim et al., 2009)
Japan	Tokai-mura	Rural	3.78	2015.10–2016.8	(Osawa et al., 2007)
Taiwan	Taichung	Urban	3.57	2014.10–2015.9	(Fang et al., 2017)
China	Beijing	Rural	3.22	2009	(Zhang et al., 2013)
China	Xiamen	Coastal	3.50	2012.3–2013.2	(Xu et al., 2015)
China	Guiyang	Urban	9.72	2009	(Fu et al., 2011)
China	Shanghai	Urban	2.70	2009	(Friedli et al., 2011)
China	Shanghai	Suburban	4.19	2014	(Duan et al., 2017b)
China	Weihai	Rural/coastal	2.31	2010	(Ci et al., 2011)
China	Chongqing	Urban	6.74	2006.8–2017.9	(Yang et al., 2009)
China	Changchun	Urban	18.40	1999.7–2000.1	(Fang et al., 2004)
China	Nanjing	Urban	7.90	2011	(Zhu et al., 2012)
China	Changbai mountain area	Rural	1.60	2008.10–2010.10	(Fu et al., 2012b)
China	Waliguan	Plateau	1.98	2007.9–2008.9	(Fu et al., 2012a)
China	Nam Co	Plateau	1.33	2012.1–2014.10	(Yin et al., 2018)
China	Ningbo	Urban	3.79	2007.10–2008.1	(Fu et al., 2012c)
China	Ningbo	Coastal	3.30	2011.4–2013.4	(Yu et al., 2015)
China	Ningbo	coastal	2.53	2016	(McLagan et al., 2018)
China	Ningbo	coastal	2.44	2016.12–2017.11	This study

Duan et al., 2017b). Table 1 summarized the results of previous studies on atmospheric mercury measurements, which indicated that the GEM concentration in Beilun was higher than those of the Arctic/Antarctic regions (0.94–1.54 ng m^{-3}) (Steffen et al., 2005; Brooks et al., 2008a; Mastromonaco et al., 2016), the remote background in Northern hemispheres (1.50–1.70 ng m^{-3}), and the rural or coastal sites at Europe and North America (1.5–2 ng m^{-3}) (Poissant et al., 2005; Choi et al., 2008; Dommergue et al., 2010; Ci et al., 2011). As to the comparison among Asia cities, the observed GEM concentration in this study was higher than those reported for Waliguan (1.98 ng m^{-3}) and Nam Co (1.33 ng m^{-3}) (Fu et al., 2012a; Yin et al., 2018), which are remote background sites in China. It was comparable to the means observed in Seoul (3.22 ng m^{-3}), Weihai (2.31 ng m^{-3}), Beijing (3.22 ng m^{-3}) (Kim et al., 2009; Ci et al., 2011; Zhang et al., 2013) and was generally lower than the values reported for Nanjing (7.90 ng m^{-3}), Shanghai (4.19 ng m^{-3}), Guiyang (9.72 ng m^{-3}) and Chongqing (6.97 ng m^{-3}) (Yang et al., 2009; Fu et al., 2011; Zhu et al., 2012; Duan et al., 2017b).

Based on the reported studies in Ningbo, the highest GEM was 3.79 ng m^{-3}, which was observed during the period of October 2007 to January 2008. The mean concentration of GEM observed in this study was 2.44 ng m^{-3}, ranking it as the lowest value among all continuous GEM measurements reported in Ningbo (Table 1) (Fu et al., 2012c; Yu et al., 2015; McLagan et al., 2018). It is known that atmospheric mercury is mainly emitted from coal combustion in China. Due to the implementation of more restrict legislation and the improvement of technology on clean coal combustion, a generally decreasing trend of coal consumption was observed from 2011 to 2017 (Fig. 2). It can be speculated that the low GEM value observed in this study was associated with the decrease in coal consumption. It should be note that a long-term monitoring of GEM at the same site is required to confirm this assumption.

3.2. Seasonal variation of GEM

The statistical summary of seasonal divided GEM is presented in Table 2. GEM concentrations in cold seasons (winter: 2.62 ± 1.05 ng m^{-3} and spring: 2.51 ± 0.87 ng m^{-3}) were

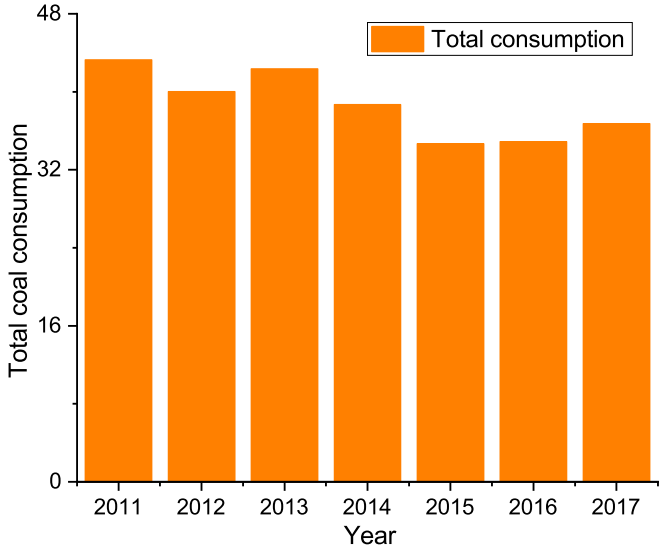

Fig. 2. Consumption of total raw coal in Ningbo from 2011 to 2017. The data in this figure were obtained from Ningbo Statistical Yearbook of 2011–2017.

Table 2
Statistical summary of seasonal mean concentrations of GEM (ng m^{-3}) at study site.

Season	Min	Max	Median	Mean	SD
Winter	0.64	10.00	2.32	2.62	1.05
Spring	1.25	9.16	2.27	2.51	0.87
Summer	0.97	10.42	2.05	2.26	0.78
Autumn	1.10	13.58	2.05	2.38	1.04
Total	0.64	13.58	2.16	2.44	0.95

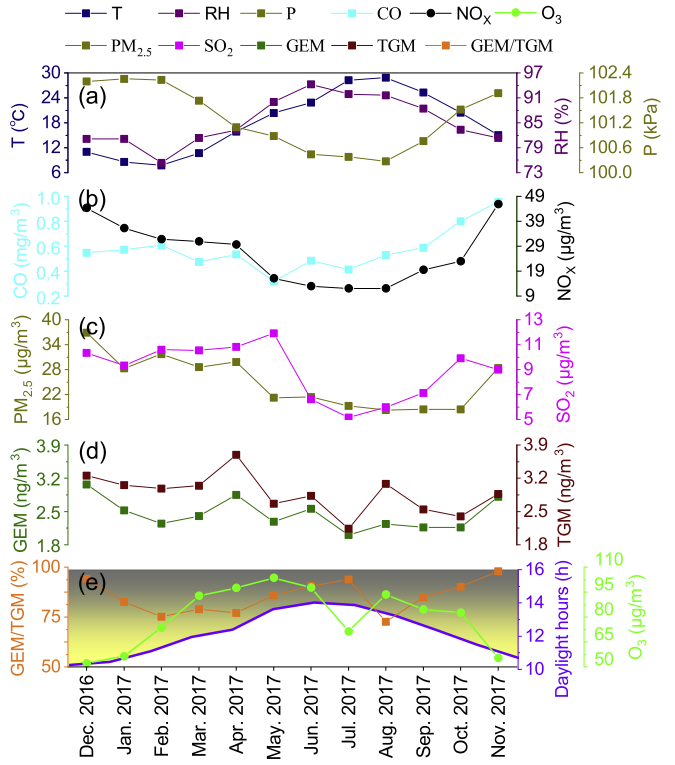

Fig. 3. Monthly variations of atmospheric mercury and other environmental variables. (a) T, P and RH, (b) CO and NO_x, (c) $PM_{2.5}$ and SO_2, (d) GEM and TGM, (e) GEM/TGM, O_3 and daylight hours.

significantly higher than those in warm seasons ($p < 0.05$, summer: 2.26 ± 0.78 ng m^{-3} and autumn: 2.38 ± 1.04 ng m^{-3}). The highest concentration typically occurs in winter and the lowest concentration occurs in summer. Similar seasonal trends were also reported in other studies (Ebinghaus et al., 2002; Ci et al., 2011). The increased coal combustion and the reduced atmospheric mixing height during the cold seasons could contribute comprehensively to the elevated atmospheric mercury levels (Kim et al., 2005). On the contrary, the higher photochemical oxidation rate of GEM in summer could reduce the GEM concentration. These might be account for the seasonal variation of GEM observed in this study.

3.3. Monthly variations of GEM, meteorological variables and ambient air pollutions

The monthly mean concentrations of GEM, meteorological variables and conventional air pollutants throughout the study period are shown in Fig. 3. Similar patterns of monthly variation were observed for both GEM and TGM. The concentrations were lower in July (GEM: 2.01 ng m^{-3}, TGM: 2.13 ng m^{-3}) with relatively high ambient temperature, RH and low air pressure. Higher GEM and TGM concentrations (Peak GEM: 3.07 ng m^{-3}, Peak TGM: 3.69 ng m^{-3}) were observed in April, November and December, which were closely related to the increasing SO_2 and $PM_{2.5}$ levels (Peak SO_2: 11.9 μg m^{-3}, Peak $PM_{2.5}$: 36.8 μg m^{-3}). GEM concentration was gradually reduced from April to July and kept stable with low concentrations (2.00–2.24 ng m^{-3}) in the later four months. The higher levels of GEM in cold seasons might be attribute to the large coal consumption at the study site. Besides, the atmospheric boundary layer height is relatively low in cold seasons compared to that in warm seasons in China (Guo et al., 2016), which might prevent the dilution of air pollutants. In contrast, the lower levels of GEM in warm seasons might be attributed to the elevated boundary layer height and improved air transport and diffusion ability of air pollutants in the warm season. During warm seasons, winds blew mainly from the sea with clean air masses significantly diluting the GEM concentration at the study site. In addition, enhanced photochemical activity in warm seasons could also accelerate the removal of GEM (Yu et al., 2015).

The monthly variation of GEM/TGM ratio was different from that of both GEM and TGM. The lowest ratio of 72.6% was observed in summer month (August) with more extended daylight hour, while a higher ratio occurred in winter. Interestingly, Fig. 3 shows that the trend of GEM/TGM ratio was roughly the opposite to that of O_3 and daylight hours. Ozone is generally the dominant oxidants for GEM (Brooks et al., 2008b). As the product of atmospheric photochemical reactions, the concentration of O3 is positively correlated to the daylight hours. Moreover, a higher level of ozone can further cause a more significant portion of GEMs to be oxidized, resulting in lower GEM/TGM ratios. It eventually contributes to the opposite trend of GEM/TGM ratio and O3 observed in this study. Both GEM/TGM ratio and O_3 exhibited two inflection points in the same months (July and August). Although the daylight hours in July were longer than those in August, the persistent rainy weather in July that accompanies the East Asian rainy season (so-called "Plum Rainy Season") can significantly reduce ozone concentrations in the atmosphere. Thus, the GEM/TGM ratio in July was 93.9%, which was about 20% higher than that in August.

3.4. Distribution of GEM in different direction

The impacts of environmental variables on air pollutants can be illustrated using the bivariate polar plot, which shows how a pollutant varies with wind conditions and other air pollutants (Paton-Walsh et al., 2017). Fig. 4a shows the relationship between GEM concentration and wind speed/direction at the study site. The directions of several source regions are identified, with higher concentrations of GEM being monitored when the site experienced strong northwest wind

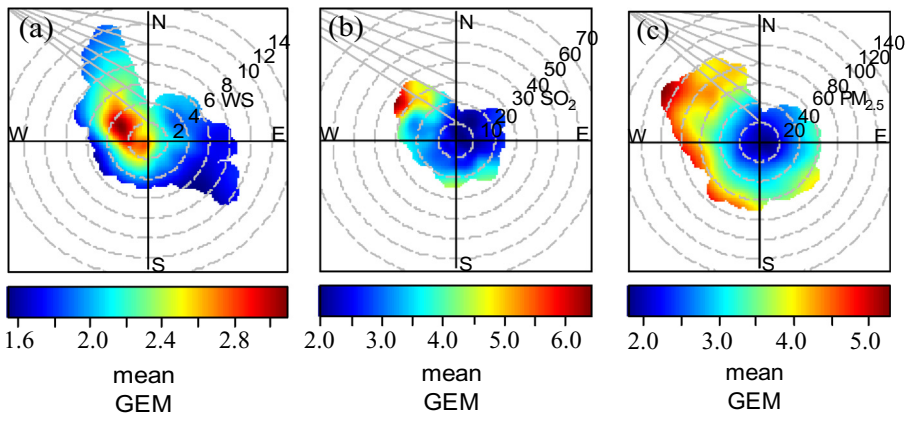

Fig. 4. Bivariate polar plot of GEM concentrations at the study site (2016.12–2017.11). The color scale shows the mean concentration of GEM in ng m^{-3} and the radial scales show (a) wind speed in m s^{-1}, (b) SO_2 in μg $m^{-3}$and (c) $PM_{2.5}$ in μg m^{-3}, which increase from the centre of the plot radially out-wards. All plots use hourly data.

(2–6 m s^{-1}) and weak southwest wind (0–2 m s^{-1}). The association of high GEM values with both high and low wind speeds indicates the influences of both regional and local sources at the study site (Grange et al., 2016). As to the regional transport, an important anthropogenic source is the Beilun coal fire power plant, which locates approximately 22 km to the northwest of the Beilun site (Fig. 1). It is the third largest coal fire power plant in China with a total installed capacity of 5000 MW. Although selective catalytic reductions, electrostatic precipitators, and wet flue gas desulfurization have been used for synergistic removal of mercury in this coal fire power plant, a considerable amount of mercury might be emitted from this plant due to large coal consumption. In addition, GEM emitted from other regional sources such as industrial boilers, domestic heating, smelting, cement production and biomass combustion could also be transported to the study site (Fu et al., 2018), which might account for the high GEM concentration under northwest winds. As to the local sources, an industrial park with many small plants, e.g. automobile manufacturing, machining, and electronic production locates on the southwest of the study site, with distance < 5 km. The industrial emissions from these plants might significantly increase the concentration of GEM under stable atmospheric conditions with low wind speeds. In contrast, very low concentrations of GEM were observed under east and northeast winds from the East China Sea. The clean air masses from the east marine area could promote the dilution of air pollutants and lead to the decrease of GEM levels at the study site. A large-scale chlor-alkali plant is located 20 km in the northeast of station, which was one of the main emission sources in the last few years. However, it has been technological transformed with mercury-free technologies, which have significantly reduced the Hg emission to the atmosphere. This might be the reason why higher GEM concentration not observed under northeast winds.

Fig. 4b shows the bivariate polar plot of GEM against SO_2. There is a strong relationship between these two species with increasing concentrations of them being observed under northwest and southwest winds. GEM and SO_2 are predominantly emitted from coal combustion. Due to the intense industrial activities in the regions to the northwest and southwest of the study area, both of the two species could be simultaneously transported to the monitoring site and contributed to the positive correlation (Fig. 4b). However, relatively low GEM was observed under varied SO_2 concentrations when east winds prevailed in the study area. This indicated that the clean air masses from the East China Sea with less mercury sources could break the close relationship between GEM and SO_2.

Similar to the relationship between GEM and SO_2, a strong positive correlation was also observed between GEM and $PM_{2.5}$, especially when the northwest and southwest winds prevailed in the study area (Fig. 4c). $PM_{2.5}$ and SO_2 have similar emission sources such as coal combustion and industrial manufacture. The high GEM concentrations that accompany with the high levels of SO_2 and $PM_{2.5}$ imply that industrial sources from northwest and southwest directions are important for GEM emission in the study region.

3.5. The variation characteristics of GEM and other environmental variables during a typical pollution episode

A typical pollution episode (lasting for 3 days) with significantly elevated GEM concentrations was observed from Dec. 21 to Dec. 24, 2016 (Fig. 5a). The hourly mean GEM concentrations steadily increased from 11:00 of Dec. 21 to 00:00 of Dec. 23 with the maximum of 6.56 ng m^{-3}, and then decreased to the minimum of 1.55 ng m^{-3} at 15:00 Dec. 24. The concentrations of GEM in the pollution period were in the range of 2.16–6.56 ng m^{-3}, with an average value of 4.08 ng m^{-3}. Before and after the period, the mean concentrations of GEM were 1.98 ng m^{-3} and 1.77 ng m^{-3}, respectively. During the pollution episode, $PM_{2.5}$ and SO_2 exhibited synchronous variations with GEM. Both GEM and $PM_{2.5}$ reached the maximum concentrations at

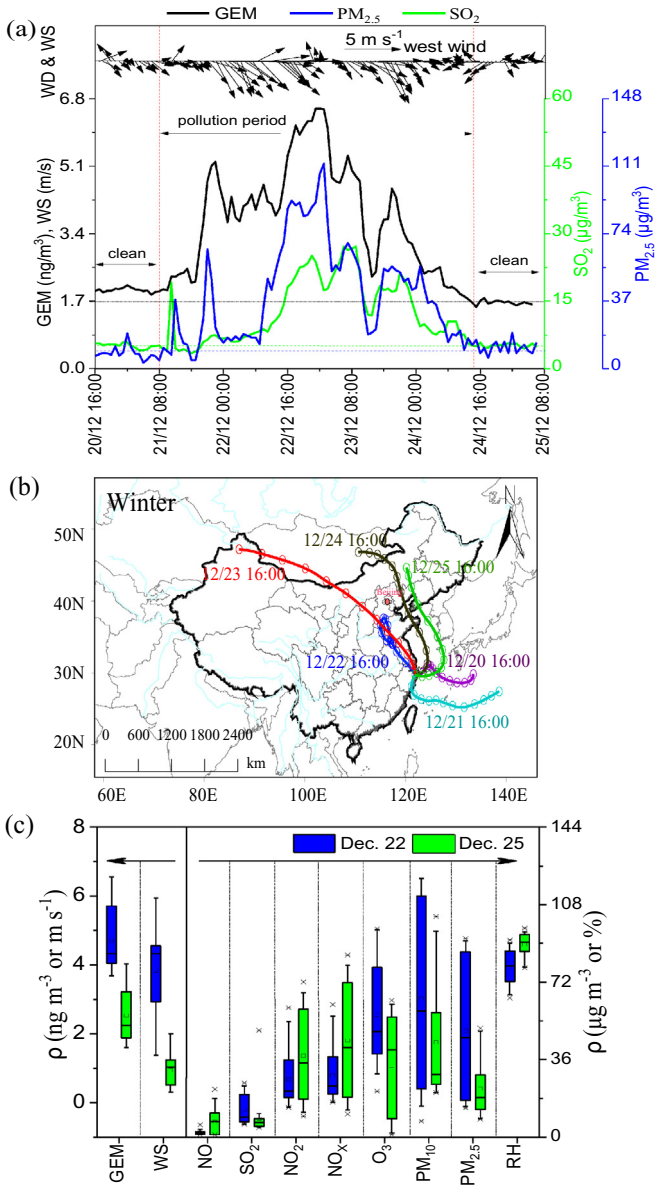

Fig. 5. (a) The variations of hourly average concentrations of GEM, $PM_{2.5}$, SO_2, wind speed and wind direction during the pollution episode from Dec. 21 to Dec. 24, 2016. (b) The calculated 72 h backward trajectories (6 h interval, starting hour: 16:00, Height: 500 m) from Dec. 20 to Dec. 25. (c) The comparison of ambient pollutant concentrations from continental air mass in Dec. 22 and those from marine air mass in Dec. 25. The arrows in the graph indicate the axis scales of the corresponding pollutants.

00:00 Dec. 23, which might be attributed to the shallow boundary layer height in the early morning (Mastromonaco et al., 2016). During the pollution episode, significant positive correlations existed between GEM and SO_2 (r = 0.756, p-value < 0.01) and $PM_{2.5}$ (r = 0.588, p-value < 0.01). It indicates that these species are likely to originate from the same source such as fossil fuel and municipal waste combustion (Liu et al., 2002; Duan et al., 2017b).

The study site is located in a coastal area of east China. This unique location provides a good opportunity to analyze the influences of oceanic and continental air masses on GEM levels (Ci et al., 2011). As shown in Fig. 5b, the 72 h backward trajectories were presented at 6 h intervals from Dec. 20 to Dec. 25 in Beilun (Zhao et al., 2015; Duan et al., 2017b). During this period, the air masses circled clockwise around the study site. The originations of the air masses changed from East China Sea during the clean period (Dec. 22-Dec. 21) to the

mainland China during the clean pollution period (Dec. 22-Dec. 24), where they might carry more ambient pollutants emitted from local anthropogenic activities to the study site. This could account for the remarkable increase of GEM, $PM_{2.5}$ and SO_2 concentrations during the pollution episode (Fig. 5a). Before and after the pollution episode (Dec. 20 and Dec. 25), the pollutant concentrations were obviously low under the influence of clean air masses from the oceanic region. A comparison of ambient pollutants during the pollution (Dec. 22) and clean periods (Dec. 25) was shown in Fig. 5c. The air mass arriving at the study site on Dec. 22 originated from the mainland of Northeast China, and passed over the Yangtze River Delta region, where considerable amounts of air pollutants were emitted from industrial activities (e.g. steel production, oil refining, cement production, industrial coating and printing) and transport (e.g. vehicle exhaust and oil evaporation) (Li et al., 2016). However, the air mass arriving on Dec. 25 came from the East China Sea where few anthropogenic sources can be identified except the maritime transport. The mean concentrations of GEM, SO_2, O_3, PM_{10} and $PM_{2.5}$ observed in the continental air masses on Dec. 22 were > 1.5 times the values observed in the marine air masses on Dec. 25. Ningbo is the third largest port city in the world with cargo throughput of 1.05 billion tons in 2017. The mean concentrations of NO_2, NO and NO_x were higher in the marine air masses. This may attribute to transportation of large container ships which emitted large amounts of NO_x.

3.6. Clustering analysis on GEM

Based on previous discussion, GEM and SO_2 probably have similar emission sources, the pollution characteristic of GEM related to SO_2 were further analyzed by K-means clustering (Fig. 6a). All the data have been classified into two categories during the study period. Cluster 1 (6875 datapoints) represents the low pollution periods, when the study site was mainly influenced by clean air masses from east marine area. The wind direction of Cluster 1 was mostly from the sector of 0°–180°. The average concentrations of GEM, SO_2, $PM_{2.5}$ for cluster 1 were 2.3 ng m^{-3}, 7.8 μg m^{-3}, 21.9 μg m^{-3}, respectively, which were obviously lower than those for cluster 2 (3.12 ng m^{-3}, 14.0 μg m^{-3}, 39.8 μg m^{-3}). The diluting effect of marine air masses on air pollutants including GEM was also confirmed in Yantai (Ci et al., 2011), Northern Europe and Mediterranean region (Wangberg et al., 2001). In comparison with cluster 1, cluster 2 represents the continental pollution sources with majority of data being recorded when westerly winds prevailed over the study site. The pollutants emitted from the continental sources were probably transported to the study site by continental air masses and contributed to the elevated GEM levels.

The ratio of GEM/TGM was 88.4% in marine air masses represented by Cluster 1, which was lower than that (92.1%) in Cluster 2. In contrast, mean concentration of O_3 (81.3 μg m^{-3}) was significantly higher than that in cluster 2 (76.3 μg m^{-3}) ($p < 0.05$). Generally, the photochemical oxidation of GEM above ocean sky plays an important role in atmospheric mercury cycling. High concentrations of O_3 in the marine air masses could enhance the oxidation of GEM to form divalent mercury via photochemical reactions (Lin et al., 2006; Huang et al., 2012) and finally decrease the GEM/TGM ratio.

Fig. 7 shows the linear regressions of GEM with SO_2 and $PM_{2.5}$, which varied with different pollutants and clusters. Relatively low values of adjusted R^2 were observed between GEM and SO_2 for both Cluster 1 ($R^2 = 0.02$, $p < 0.05$) and Cluster 2 ($R^2 = 0.14$, $p < 0.05$) (Fig. 7a and b). The slopes of the regression lines were exhibited large discrepancy between cluster 1 and cluster 2. This may be explained by the higher reactivity and shorter residence time of SO_2 in the atmosphere compared with those of GEM (Duan et al., 2017b). The SO_2 concentration may significantly decrease before it arriving at the study site. In contrast, GEM and $PM_{2.5}$ were relatively well correlated in the two clusters ($R^2 = 0.37$–0.45, $p < 0.05$) (Fig. 7c and d). The variation pattern of $PM_{2.5}$ is different from SO_2, which is gradually decreased without the additional input of SO_2. It can be gradually generated by secondary reaction during the transportation process, and counteract the air dilution effect. The slopes of the regression lines were similar for Cluster 1 (0.03) and Cluster 2 (0.04), which are stable and may not influence by the source classification.

3.7. Backward trajectories analysis

In this study, a concentration weighted trajectory analysis (CWT) is used to reveal the potential GEM sources at Beilun (Fig. 8). During the whole study period (Fig. 8a), the main source regions of GEM lies in the border areas among southern Anhui, eastern Hubei and northern Jiangxi (red areas in Fig. 8a). The GEM loadings are also very high in eastern Jiangxi and central Anhui. These provinces are developed in non-ferrous metal smelting and coal producing, with large amounts of mercury being emitted into the atmosphere annually. Previous studies estimated that the annual emissions of total Hg in Anhui, Hubei and Jiangxi were 14.56, 15.95 and 9.64 t, respectively (Streets et al., 2005; Fu et al., 2012b). Therefore, long-range transport of mercury from these regions might play an important role in enhancing the concentration of GEM at the study site.

The long-range transportation in the study site from Chinese heavy

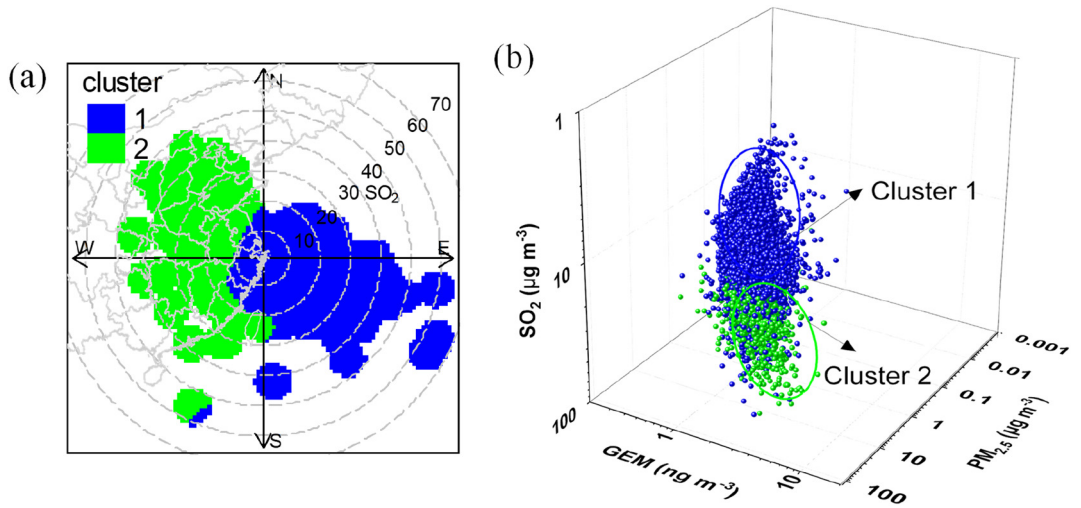

Fig. 6. Two clusters identified for GEM at the study site by k-means clustering. (a) k-means clustering plot (b) The distribution of GEM, SO_2 and $PM_{2.5}$ after k-means clustering.

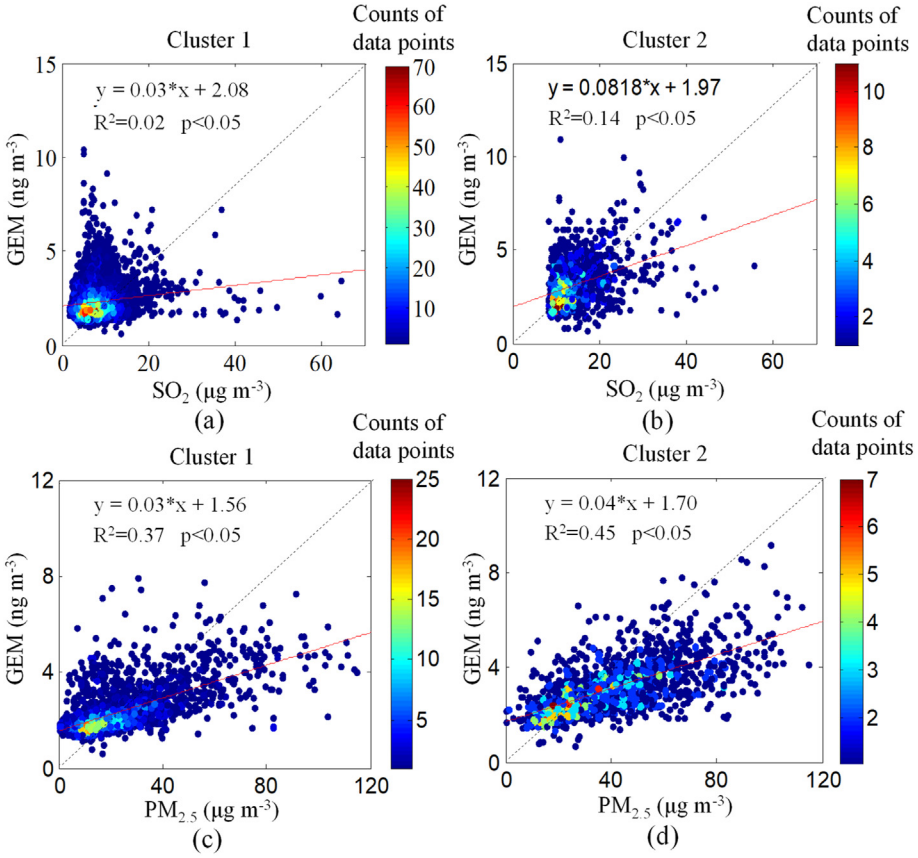

Fig. 7. Linear regressions between GEM and SO_2 ((a) and (b)) and $PM_{2.5}$ ((c) and (d)) for the two clusters at the monitoring site from Dec. 2016 to Nov. 2017. The dashed line is the 1:1 line.

mercuric polluted regions (such as Guizhou province) are lower than that from Yangtze River Delta region and middle China. The contributions of long-range transport from Russia, Korea and Japan were very low due to the dilution effect (Tan et al., 2000). Taken in total, the main potential sources for GEM in Beilun are mainly impacted by coastal provinces (Fujian, Jiangsu and Zhejiang) and inland provinces (Jiangxi, Anhui and Hubei) which have high GEM loading. In addition, the GEM loading of the airflow from the East China Sea was lower than those of other directions, indicating that the dilution of marine airflow and enhanced oxidation of GEM over the sea are important for GEM depletion in coastal area.

In winter, high GEM loadings ($> 3.6\,ng\,m^{-3}$) were found in northwest and north of Zhejiang Province (Fig. 8b), where many industrial enterprises and coal fire power plants were built. A considerable amount of mercury might be emitted from local industrial activities, and finally contribute to the atmospheric GEM pollution at the study area via regional transport of air pollutants. This finding agreed well with the previous studies which observed high GEM loadings over the Yangtze River Delta region (Ci et al., 2011; Duan et al., 2017b; Tang et al., 2018). The transport of GEM from other province is relatively lower, which indicated that the influence of local and regional sources is higher than that from long-range sources in winter.

A noticeable change in source contribution for GEM was observed in spring with GEM loadings basically lower than $2.8\,ng\,m^{-3}$ (Fig. 8c), which was lower compared with other seasons. During the summertime, high GEM loadings ($> 3.6\,ng\,m^{-3}$) were found in the northeastern Jiangxi, southern Anhui and northern Zhejiang (Fig. 8d). However, during the summer monsoon season, the dominant wind direction was from East China Sea, where most of GEM loading in this region were below $2.40\,ng\,m^{-3}$, the average GEM concentration is the lowest ($2.26\,ng\,m^{-3}$) during the summertime.

There are two regions with high GEM loadings ($> 3.6\,ng\,m^{-3}$) identified in Autumn by CWT. The first one is located in the border areas among Anhui, Hubei and Jiangxi provinces, which indicated the exist of distant mercury sources (Fig. 8e). The other one is located in Yangtze River Delta region, including the southern Jiangsu, Shanghai and northern Zhejiang, which indicated the local and regional sources. Both of them could comprehensively contribute to the relatively high average GEM ($2.38\,ng\,m^{-3}$) observed in autumn.

4. Conclusion

In order to investigate the characteristics of atmospheric mercury in east China, GEM as well as other air pollutants were continuously measured at a coastal site in Ningbo, China from December 2016 to November 2017. Relatively low level of GEM was observed compared to those of other Asian cities. The atmospheric GEM exhibited obvious seasonal variations, with the highest concentration in winter and the lowest value in summer, respectively. Similar trends of variation were found between GEM and SO_2 and $PM_{2.5}$, especially during the pollution episode, which indicated that the atmospheric mercury in the study area probably had similar sources (e.g. coal-fire power plants). The rate of photochemical oxidation of GEM by O_3 is positively correlated to the daylight hour, lower O_3 concentration hindered the transformation of GEM into oxidation products. GEM levels in the air masses originating from the continental region were significantly higher than those from the marine region. Based on the bivariate polar plot and CWT analysis, GEM at the study site was found to be strongly contributed by the regional transport of air pollutants from northern Zhejiang and southern Jiangsu. Coordinated inter-regional control on source emissions are critical to the mercury reduction in the study area.

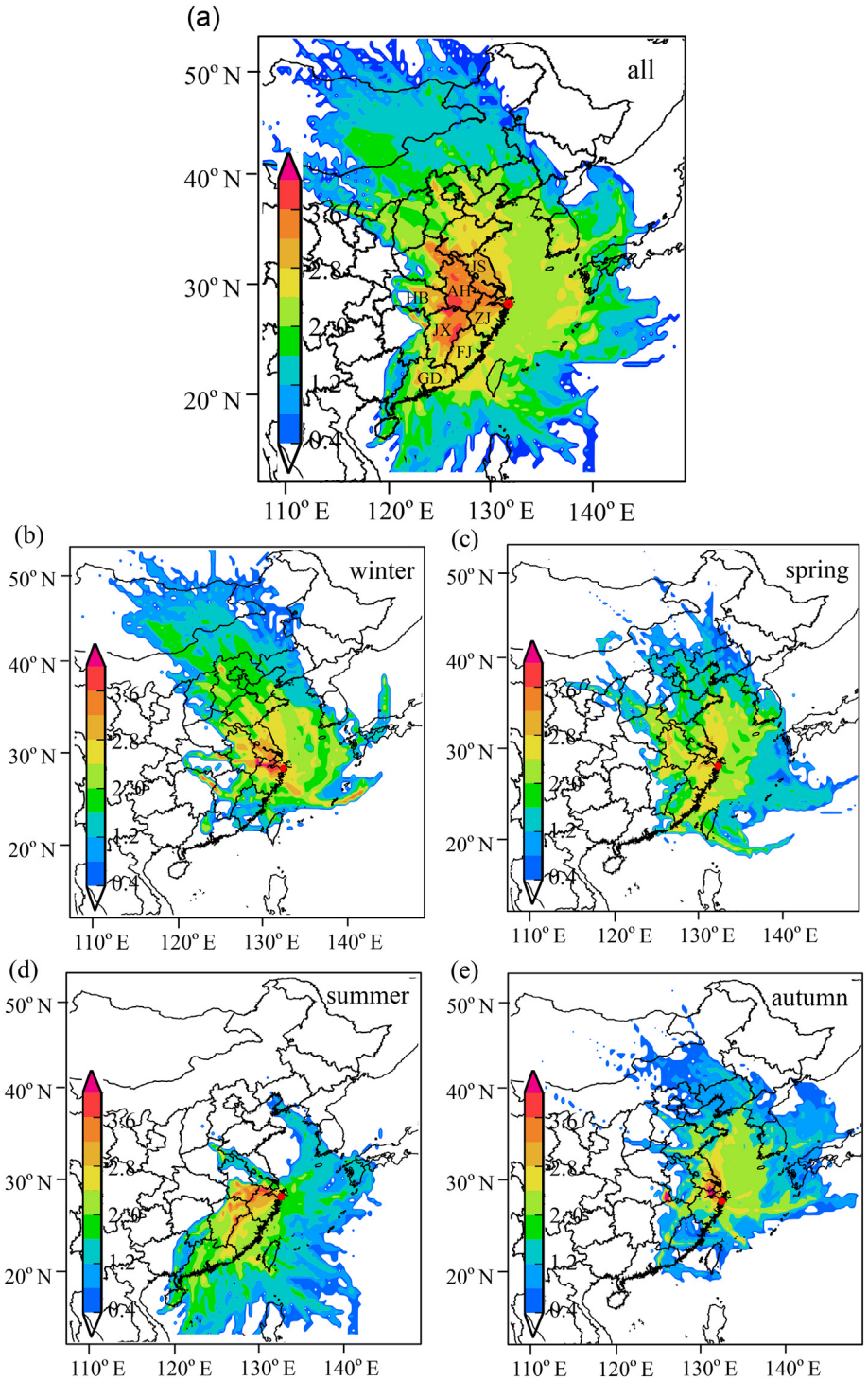

Fig. 8. Smoothed maps of GEM concentration weighted trajectory (CWT) at 500 m altitude at the study site (red circle) for (a) the whole study period, (b) winter, (c) spring, (d) summer, and (e) autumn (ZJ: Zhejiang province, JS: Jiangsu province, FJ: Fujian province, JX: Jiangxi province, AH: Anhui province, HB: Hubei province, GD: Guangdong province). (For interpretation of the references to color in this figure legend, the reader is referred to the web version of this article.)

Funding

This work was supported by the National Natural Science Foundation of China (No. 41575146, 21507127, 31300435), Science and Technology Plan Project of Ningbo City (grant number 2015C110001) and Natural Science Foundation of Ningbo City (grant number 2015A610247).

References

Brooks, S., Arimoto, R., Lindberg, S., Southworth, G., 2008a. Antarctic polar plateau snow surface conversion of deposited oxidized mercury to gaseous elemental mercury with fractional long-term burial. Atmos. Environ. 42 (12), 2877–2884. https://doi.org/10.1016/j.atmosenv.2007.05.029.

Brooks, S., Lindberg, S., Southworth, G., Arimoto, R., 2008b. Springtime atmospheric mercury speciation in the McMurdo, Antarctica coastal region. Atmos. Environ. 42 (12), 2885–2893. https://doi.org/10.1016/j.atmosenv.2007.06.038.

Carslaw, D.C., Beevers, S.D., 2013. Characterising and understanding emission sources using bivariate polar plots and k-means clustering. Environ. Model. Softw. 40,

325–329. https://doi.org/10.1016/j.envsoft.2012.09.005.
Carslaw, D.C., Ropkins, K., 2012. Openair - an R package for air quality data analysis. Environ. Model. Softw. 27, 52–61. https://doi.org/10.1016/j.envsoft.2011.09.008.
Choi, H.D., Holsen, T.M., Hopke, P.K., 2008. Atmospheric mercury (Hg) in the Adirondacks: concentrations and sources. Environ. Sci. Technol. 42 (15), 5644–5653. https://doi.org/10.1021/es7028137.
Choi, H.D., Huang, J.Y., Mondal, S., Holsen, T.M., 2013. Variation in concentrations of three mercury (Hg) forms at a rural and a suburban site in New York State. Sci. Total Environ. 448, 96–106. https://doi.org/10.1016/j.scitotenv.2012.08.052.
Chuang, H.C., Shie, R.H., Chio, C.P., Yuan, T.H., Lee, J.H., 2018. Cluster analysis of fine particulate matter ($PM_{2.5}$) emissions and its bioreactivity in the vicinity of a petrochemical complex. Environ. Pollut. 236, 591–597. https://doi.org/10.1016/j.envpol.2018.01.067.
Ci, Z.J., Zhang, X.S., Wang, Z.W., Niu, Z.C., 2011. Atmospheric gaseous elemental mercury (GEM) over a coastal/rural site downwind of East China: temporal variation and long-range transport. Atmos. Environ. 45 (15), 2480–2487. https://doi.org/10.1016/j.atmosenv.2011.02.043.
Dommergue, A., Sprovieri, F., Pirrone, N., Ebinghaus, R., Brooks, S., 2010. Overview of mercury measurements in the Antarctic troposphere. Atmos. Chem. Phys. 10 (7), 3309–3319. https://doi.org/10.5194/acp-10-3309-2010.
Duan, L., Cheng, N., Xiu, G.L., Wang, F.J., Chen, Y., 2017a. Characteristics and source appointment of atmospheric particulate mercury over East China Sea: implication on the deposition of atmospheric particulate mercury in marine environment. Environ. Pollut. 224, 26–34. https://doi.org/10.1016/j.envpol.2016.10.103.
Duan, L., Wang, X.H., Wang, D.F., Duan, Y.S., Cheng, N., 2017b. Atmospheric mercury speciation in Shanghai, China. Sci. Total Environ. 578, 460–468. https://doi.org/10.1016/j.scitotenv.2016.10.209.
Ebinghaus, R., Kock, H.H., Schmolke, S.R., 2001. Measurements of atmospheric mercury with high time resolution: recent applications in environmental research and monitoring. Fresenius J. Anal. Chem. 371 (6), 806–815. https://doi.org/10.1007/s002160101048.
Ebinghaus, R., Kock, H.H., Coggins, A.M., Spain, T.G., Jennings, S.G., 2002. Long-term measurements of atmospheric mercury at Mace Head, Irish west coast, between 1995 and 2001. Atmos. Environ. 36 (34), 5267–5276. https://doi.org/10.1016/S1352-2310(02)00691-X.
Fang, F.M., Wang, Q.C., Li, J.F., 2004. Urban environmental mercury in Changchun, a metropolitan city in Northeastern China: source, cycle, and fate. Sci. Total Environ. 330 (1–3), 159–170. https://doi.org/10.1016/j.scitotenv.2004.04.006.
Fang, G.C., Lo, C.T., Cho, M.H., Zhuang, Y.J., Tsai, K.H., 2017. Annual ambient atmospheric mercury speciation measurement from Longjing, a rural site in Taiwan. Environ. Geochem. Health 39 (4), 901–911. https://doi.org/10.1007/s10653-016-9861-x.
Friedli, H.R., Arellano, A.F., Geng, F., Cai, C., Pan, L., 2011. Measurements of atmospheric mercury in Shanghai during September 2009. Atmos. Chem. Phys. 11 (8), 3781–3788. https://doi.org/10.5194/acp-11-3781-2011.
Fu, X.W., Feng, X., Dong, Z.Q., Yin, R.S., Wang, J.X., 2010. Atmospheric gaseous elemental mercury (GEM) concentrations and mercury depositions at a high-altitude mountain peak in south China. Atmos. Chem. Phys. 10 (5), 2425–2437. https://doi.org/10.5194/acp-10-2425-2010.
Fu, X.W., Feng, X.B., Qiu, G.L., Shang, L.H., Zhang, H., 2011. Speciated atmospheric mercury and its potential source in Guiyang, China. Atmos. Environ. 45 (25), 4205–4212. https://doi.org/10.1016/j.atmosenv.2011.05.012.
Fu, X.W., Feng, X., Liang, P., Deliger, Zhang, H., Ji, J., Liu, P., 2012a. Temporal trend and sources of speciated atmospheric mercury at Waliguan GAW station, Northwestern China. Atmos. Chem. Phys. 12 (4), 1951–1964. https://doi.org/10.5194/acp-12-1951-2012.
Fu, X.W., Feng, X., Shang, L.H., Wang, S.F., Zhang, H., 2012b. Two years of measurements of atmospheric total gaseous mercury (TGM) at a remote site in Mt. Changbai area, Northeastern China. Atmos. Chem. Phys. 12 (9), 4215–4226. https://doi.org/10.5194/acp-12-4215-2012.
Fu, X.W., Feng, X.B., Sommar, J., Wang, S.F., 2012c. A review of studies on atmospheric mercury in China. Sci. Total Environ. 421, 73–81. https://doi.org/10.1016/j.scitotenv.2011.09.089.
Fu, X.W., Yang, X., Tan, Q.Y., Ming, L.L., Lin, T., Lin, C.J., Li, X.D., Feng, X.B., 2018. Isotopic composition of gaseous elemental mercury in the boundary layer of East China Sea. J. Geophys. Res.-Atmos. 123 (14), 7656–7669. https://doi.org/10.1029/2018jd028671.
Grange, S.K., Lewis, A.C., Carslaw, D.C., 2016. Source apportionment advances using polar plots of bivariate correlation and regression statistics. Atmos. Environ. 145, 128–134. https://doi.org/10.1016/j.atmosenv.2016.09.016.
Guo, J.P., Miao, Y.C., Zhang, Y., Liu, H., Li, Z.Q., Zhang, W.C., He, J., Lou, M.Y., Yan, Y., Bian, L.G., Zhai, P., 2016. The climatology of planetary boundary layer height in China derived from radiosonde and reanalysis data. Atmos. Chem. Phys. 16 (20), 13309–13319. https://doi.org/10.5194/acp-16-13309-2016.
Hall, B., 1995. The gas-phase oxidation of elemental mercury by ozone. Water Air Soil Pollut. 80 (1–4), 301–315. https://doi.org/10.1007/Bf01189680.
Holmes, C.D., Jacob, D.J., Corbitt, E.S., Mao, J., Yang, X., Talbot, R., Slemr, F., 2010. Global atmospheric model for mercury including oxidation by bromine atoms. Atmos. Chem. Phys. 10 (24), 12037–12057.
Huang, J.Y., Liu, C.K., Huang, C.S., Fang, G.C., 2012. Atmospheric mercury pollution at an urban site in Central Taiwan: mercury emission sources at ground level. Chemosphere 87 (5), 579–585. https://doi.org/10.1016/j.chemosphere.2012.01.011.
Jones, A.M., Harrison, R.M., Baker, J., 2010. The wind speed dependence of the concentrations of airborne particulate matter and NOx. Atmos. Environ. 44 (13), 1682–1690. https://doi.org/10.1016/j.atmosenv.2010.01.007.
Kim, K.H., Ebinghaus, R., Schroeder, W.H., Blanchard, P., Kock, H.H., 2005. Atmospheric mercury concentrations from several observatory sites in the northern hemisphere. J. Atmos. Chem. 50 (1), 1–24. https://doi.org/10.1007/s10874-005-9222-0.
Kim, S.H., Han, Y.J., Holsen, T.M., Yi, S.M., 2009. Characteristics of atmospheric speciated mercury concentrations (TGM, Hg(II) and Hg(p)) in Seoul, Korea. Atmos. Environ. 43 (20), 3267–3274. https://doi.org/10.1016/j.atmosenv.2009.02.038.
Li, L., An, J.Y., Shi, Y.Y., Zhou, M., Yan, R.S., 2016. Source apportionment of surface ozone in the Yangtze River Delta, China in the summer of 2013. Atmos. Environ. 144, 194–207. https://doi.org/10.1016/j.atmosenv.2016.08.076.
Lin, C.J., Pongprueksa, P., Lindberg, S.E., Pehkonen, S.O., Byun, D., 2006. Scientific uncertainties in atmospheric mercury models I: model science evaluation. Atmos. Environ. 40 (16), 2911–2928. https://doi.org/10.1016/j.atmosenv.2006.01.009.
Liu, S.L., Nadim, F., Perkins, C., Carley, R.J., Hoag, G.E., 2002. Atmospheric mercury monitoring survey in Beijing, China. Chemosphere 48 (1), 97–107. https://doi.org/10.1016/S0045-6535(02)00026-7.
Liu, B., Keeler, G.J., Dvonch, J.T., Barres, J.A., Lynam, M.M., 2010. Urban-rural differences in atmospheric mercury speciation. Atmos. Environ. 44 (16), 2013–2023. https://doi.org/10.1016/j.atmosenv.2010.02.012.
Mastromonaco, M.N., Gardfeldt, K., Jourdain, B., Abrahamsson, K., Granfors, A., 2016. Antarctic winter mercury and ozone depletion events over sea ice. Atmos. Environ. 129, 125–132. https://doi.org/10.1016/j.atmosenv.2016.01.023.
McLagan, D.S., Mitchell, C.P.J., Steffen, A., Hung, H., Shin, C., 2018. Global evaluation and calibration of a passive air sampler for gaseous mercury. Atmos. Chem. Phys. 18 (8), 5905–5919. https://doi.org/10.5194/acp-18-5905-2018.
Ningbo Municipal Statistics Bureau, 2018. Statistical Yearbook of Ningbo 2017. China Statistical Press, Beijing (in Chinese).
Osawa, T., Ueno, T., Fu, F.F., 2007. Sequential variation of atmospheric mercury in Tokaimura, seaside area of eastern central Japan. J. Geophys. Res. Atmos. 112 (D19), 1–9. https://doi.org/10.1029/2007JD008538.
Pankratov, F.F., Konoplev, A.V., Makhura, A., Kats, O.V., 2013. Analysis of the data of long-term monitoring of atmospheric mercury content and meteorological parameters at Amderma polar station. Russ. Meteorol. Hydrol. 38 (6), 405–413. https://doi.org/10.3103/S1068373913060058.
Paton-Walsh, C., Guerette, E.A., Kubistin, D., Humphries, R., Wilson, S.R., 2017. The MUMBA campaign: measurements of urban, marine and biogenic air. Earth Syst. Sci. Data 9 (1), 349–362. https://doi.org/10.5194/essd-9-349-2017.
Poissant, L., Pilote, M., Beauvais, C., Constant, P., Zhang, H.H., 2005. A year of continuous measurements of three atmospheric mercury species (GEM, RGM and Hg-p) in southern Quebec, Canada. Atmos. Environ. 39 (7), 1275–1287. https://doi.org/10.1016/j.atmosenv.2004.11.007.
Polissar, A.V., Hopke, P.K., Paatero, P., Kaufmann, Y.J., Hall, D.K., 1999. The aerosol at Barrow, Alaska: long-term trends and source locations. Atmos. Environ. 33 (16), 2441–2458. https://doi.org/10.1016/S1352-2310(98)00423-3.
Schneider, L., Mariani, M., Saunders, K.M., Maher, W.A., Harrison, J.J., 2019. How significant is atmospheric metal contamination from mining activity adjacent to the Tasmanian Wilderness World Heritage Area? A spatial analysis of metal concentrations using air trajectories models. Sci. Total Environ. 656, 250–260. https://doi.org/10.1016/j.scitotenv.2018.11.241.
Schroeder, W.H., Munthe, J., 1998. Atmospheric mercury - An overview. Atmos. Environ. 32 (5), 809–822. https://doi.org/10.1016/S1352-2310(97)00293-8.
Steffen, A., Schroeder, W., Macdonald, R., Poissant, L., Konoplev, A., 2005. Mercury in the Arctic atmosphere: an analysis of eight years of measurements of GEM at Alert (Canada) and a comparison with observations at Amderma (Russia) and Kuujjuarapik (Canada). Sci. Total Environ. 342 (1–3), 185–198. https://doi.org/10.1016/j.scitotenv.2004.12.048.
Streets, D.G., Hao, J.M., Wu, Y., Jiang, J.K., Chan, M., Tian, H.Z., Feng, X.B., 2005. Anthropogenic mercury emissions in China. Atmos. Environ. 39, 7789–7806. https://doi.org/10.1016/j.atmosenv.2005.08.029.
Tan, H., He, J.L., Liang, L., Lazoff, S., Sommer, J., 2000. Atmospheric mercury deposition in Guizhou, China. Sci. Total Environ. 259 (1–3), 223–230. https://doi.org/10.1016/S0048-9697(00)00584-2.
Tang, Y., Wang, S.X., Wu, Q.R., Liu, K.Y., Wang, L., 2018. Recent decrease trend of atmospheric mercury concentrations in East China: the influence of anthropogenic emissions. Atmos. Chem. Phys. 18 (11), 8279–8291. https://doi.org/10.5194/acp-18-8279-2018.
Wang, Y.Q., Zhang, X.Y., Draxler, R.R., 2009. TrajStat: GIS-based software that uses various trajectory statistical analysis methods to identify potential sources from long-term air pollution measurement data. Environ. Model. Softw. 24 (8), 938–939. https://doi.org/10.1016/j.envsoft.2009.01.004.
Wang, C.J., Wang, Z.W., Ci, Z.J., Zhang, X.S., Tang, X., 2016. Spatial-temporal distributions of gaseous element mercury and particulate mercury in the Asian marine boundary layer. Atmos. Environ. 126, 107–116. https://doi.org/10.1016/j.atmosenv.2015.11.036.
Wangberg, I., Munthe, J., Pirrone, N., Iverfeldt, A., Bahlman, E., 2001. Atmospheric mercury distribution in Northern Europe and in the Mediterranean region. Atmos. Environ. 35 (17), 3019–3025. https://doi.org/10.1016/S1352-2310(01)00105-4.
Westmoreland, E.J., Carslaw, N., Carslaw, D.C., Gillah, A., Bates, E., 2007. Analysis of air quality within a street canyon using statistical and dispersion modelling techniques. Atmos. Environ. 41 (39), 9195–9205. https://doi.org/10.1016/j.atmosenv.2007.07.057.
Xu, L.L., Chen, J.S., Yang, L.M., Niu, Z.C., Tong, L., 2015. Characteristics and sources of atmospheric mercury speciation in a coastal city, Xiamen, China. Chemosphere 119, 530–539. https://doi.org/10.1016/j.chemosphere.2014.07.024.
Yang, Y.K., Chen, H., Wang, D.Y., 2009. Spatial and temporal distribution of gaseous elemental mercury in Chongqing, China. Environ. Monit. Assess. 156 (1–4), 479–489. https://doi.org/10.1007/s10661-008-0499-8.

Yin, X.F., Kang, S.C., de Foy, B., Ma, Y.M., Tong, Y.D., Zhang, W., Wang, X.J., Zhang, G.S., Zhang, Q.G., 2018. Multi-year monitoring of atmospheric total gaseous mercury at a remote high-altitude site (Nam Co, 4730 m a.s.l.) in the inland Tibetan Plateau region. Atmos. Chem. Phys. 18 (14), 10557–10574. https://doi.org/10.5194/acp-18-10557-2018.

Ying, H., Deng, M.H., Li, T.Q., Jan, J.P.G., Chen, Q.Q., 2017. Anthropogenic mercury emissions from 1980 to 2012 in China. Environ. Pollut. 226, 230–239. https://doi.org/10.1016/j.envpol.2017.03.059.

Yu, B., Wang, X., Lin, C.J., Fu, X.W., Zhang, H., 2015. Characteristics and potential sources of atmospheric mercury at a subtropical near-coastal site in East China. J. Geophys. Res. Atmos. 120 (16), 8563–8574. https://doi.org/10.1002/2015jd023425.

Zhang, L., Wang, S.X., Wang, L., Hao, J.M., 2013. Atmospheric mercury concentration and chemical speciation at a rural site in Beijing, China: implications of mercury emission sources. Atmos. Chem. Phys. 13 (20), 10505–10516. https://doi.org/10.5194/acp-13-10505-2013.

Zhao, M.F., Huang, Z.S., Qiao, T., Zhang, Y.K., Xiu, G.L., 2015. Chemical characterization, the transport pathways and potential sources of $PM_{2.5}$ in Shanghai: seasonal variations. Atmos. Res. 158, 66–78. https://doi.org/10.1016/j.atmosres.2015.02.003.

Zhu, J., Wang, T., Talbot, R., Mao, H., Hall, C.B., 2012. Characteristics of atmospheric Total Gaseous Mercury (TGM) observed in urban Nanjing, China. Atmos. Chem. Phys. 12 (24), 12103–12118. https://doi.org/10.5194/acp-12-12103-2012.